



HAL
open science

Superhard hexagonal sp^3 -bonded BN polytypes and BC₂N from crystal chemistry and first principles

Samir F. Matar, Vladimir Solozhenko

► **To cite this version:**

Samir F. Matar, Vladimir Solozhenko. Superhard hexagonal sp^3 -bonded BN polytypes and BC₂N from crystal chemistry and first principles. *Journal of Superhard Materials*, 2024, 46 (2), pp.81-93. 10.3103/S1063457624020060 . hal-04190356

HAL Id: hal-04190356

<https://hal.science/hal-04190356>

Submitted on 29 Aug 2023

HAL is a multi-disciplinary open access archive for the deposit and dissemination of scientific research documents, whether they are published or not. The documents may come from teaching and research institutions in France or abroad, or from public or private research centers.

L'archive ouverte pluridisciplinaire **HAL**, est destinée au dépôt et à la diffusion de documents scientifiques de niveau recherche, publiés ou non, émanant des établissements d'enseignement et de recherche français ou étrangers, des laboratoires publics ou privés.




Distributed under a Creative Commons Attribution 4.0 International License


Superhard hexagonal sp^3 -bonded BN polytypes and BC_2N from crystal chemistry and first principles

Samir F. Matar¹ and Vladimir L. Solozhenko^{2,*}

¹ Lebanese German University, Jounieh, P.O. Box 206, Lebanon

 <https://orcid.org/0000-0001-5419-358X>

² LSPM–CNRS, Université Sorbonne Paris Nord, 93430 Villetaneuse, France

 <https://orcid.org/0000-0002-0881-9761>

Abstract

*In the framework of a crystallochemical approach, new hexagonal ($P6_3/mc$) sp^3 -bonded BN polytypes (4H, 6H and 8H) and ternary BC_2N were proposed by rationalized substitutions of C for B and N in hexagonal carbon allotrope C_8 (4C carbon) with **cfc** topology, and density functional theory calculations of their ground states were performed. All new phases were found to be cohesive and stable mechanically (elastic constants) and dynamically (phonon band structures). According to modern models of hardness, the new phases were recognized as superhard with Vickers hardness above 50 GPa. Their electronic band structures exhibit insulating behavior with large band gaps.*

Keywords: BN polytypes; BC_2N ; DFT; crystal structure; hardness; phonons; band structures

* Corresponding author (e-mail: vladimir.solozhenko@univ-paris13.fr)

Introduction

The properties of diamond, in particular its exceptional hardness but relatively low thermal stability, have prompted numerous experimental and theoretical studies aimed at finding substitutes for diamond, both in abrasives and tools, as well as in electronics and other applications. In this respect, the search for new binary and ternary superhard refractory phases of compounds of light elements (especially in the B-C-N system) seems to be the most promising [1,2].

Diamond occurs in two forms, the common cubic ($Fd-3m$) and the relatively rare hexagonal ($P6_3/mmc$) (the so-called "lonsdaleite"), which are referred to as polytypes 3C and 2H, respectively. From the point of view of topology, these polytypes are referred to as **dia** and **lon** [3].

An enormous number of polytype crystal structures are known for silicon carbide, SiC, with the most well known being **cfc** 6H ($P6_3/mc$) "moissanite". The **cfc** topology is also adopted by hexagonal carbon allotrope C_8 , called "4C carbon" [4], which is used here to create new BN and BC_2N structures.

BN is isoelectronic with two carbon atoms $BN(8e) \equiv 2C(8e)$ (e = electron) and is known to exist in four polymorphic modifications: two graphite-like, hexagonal ($P6_3/mm$) (hBN) and rhombohedral ($R3m$) (rBN), and two dense, cubic ($F-43m$) (cBN) and wurtzite ($P6_3/mc$) (wBN), which are close analogs of the main carbon allotropes (hexagonal and rhombohedral graphite, diamond and lonsdaleite). BN it is also isoelectronic with SiC: $BN(8e) \equiv SiC(8e)$. The eight electrons belong to the outer shells, i.e. $2s^2, 2p^n$ for the second period elements B, C, N ($n = 1, 2$ and 3 , respectively) and $3s^2, 3p^2$ for the third period element Si.

It should be noted that for boron nitride mainly sp^2 -bonded polytypes are known, which are characterized by different layer stacking sequences (e.g. $AA'AA'$ for hexagonal BN, $ABCABC$ for rhombohedral BN, etc.) [5]. In our work results on new hexagonal sp^3 -bonded BN polytypes and BC_2N with **cfc** topology are presented. The studies of the structures of the new phases based on crystallochemical "engineering" are supported by data on their stability, mechanical and dynamic properties, and structure of electronic bands, all calculated in the quantum mechanics framework of the Density Functional Theory (DFT) [6,7].

Computational framework

All devised structural setups have been subjected to unconstrained geometry relaxations of atomic positions and lattice constants down to the ground states characterized by minimum energies. The protocol consists of successive iterative cycles with increasing precision of the Brillouin zone (BZ) k-mesh in the reciprocal lattice. The calculations were performed using the DFT-based plane-wave Vienna Ab initio Simulation Package (VASP) [8,9]. The projector augmented wave (PAW) method was used for the atomic potentials [9,10]. The exchange X and correlation effects (XC) were treated within a Generalized Gradient Approximation (GGA) scheme [11]. Test calculations with the hybrid functional HSE06 [12] did not lead to better results than GGA. The relaxation of the atoms

to the ground state geometry was performed using a conjugate-gradient algorithm [13]. Blöchl tetrahedron method [14] with corrections according to Methfessel and Paxton scheme [15] was used for geometry optimization and energy calculations. A special k -point sampling [16] was used to approximate the BZ reciprocal space integrals. For better reliability, the optimization of the structural parameters was carried out along with successive self-consistent cycles with increasing k -mesh until the forces on atoms were less than 0.02 eV/Å and the stress components were less than 0.003 eV/Å³.

Mechanical stability and hardness were estimated from the calculated elastic constants [17]. The phonon dispersion band structures were calculated to verify the dynamic stability of the new phases. The phonon modes were computed considering the harmonic approximation by finite displacements of the atoms around their equilibrium positions to obtain the forces from the summation over the different configurations. The phonon dispersion curves along the direction of the Brillouin zone were then obtained using "Phonopy" interface code [18]. The crystal structure sketches and charge density projections were generated using the VESTA graphics software [19]. The electronic band structures and densities of states were obtained with the full-potential augmented spherical wave ASW method based on DFT using the same GGA scheme as above [20].

Crystal chemistry

Octacarbon C₈ with **cfc** topology structure shown in Fig. 1a belongs to hexagonal space group $P6_3/mmc$ (No. 194) with two different 4-fold Wyckoff positions for carbon. Table 1 shows that the presently calculated structure parameters of C₈ are in good agreement with the literature data [4] given in brackets. Note that lonsdaleite C₄ (**lon** topology) crystallizing in the same space group has a single 4-fold carbon position, (4f) 2/3, 1/3, 0.06250, with lattice parameters $a = 2.52$ Å and $c = 4.12$ Å [21]. The calculated atom-averaged cohesive energy of C₈ is the same as that of diamond and lonsdaleite, i.e. $E_{\text{coh}}/\text{atom} = -2.49$ eV. In both space groups the interatomic distance $d(\text{C-C})$ is the same, 1.54 Å.

A straightforward, preliminary, substitution scheme based on the high-symmetry structure with B at (4a) and N at (4f) resulted in energetically unfavorable configuration due to the presence of B-B and N-N bonds. The description of the structure in a lower symmetry space group $P6_3mc$, No. 186 (the same space group as that of wBN) was then carried out resulting in four 2-fold atomic positions (2a) and (2b) as shown in the 2nd data column of Table 1. As a result, the same cohesive energy and close lattice parameters were found for this structure template, which now allows substitutional sites to be occupied by B and N, avoiding unfavorable bonds between atoms of the same chemical nature. The obtained BN structure with 4 formula units (Z) in the unit cell is shown in Fig. 1b; the structure parameters are given in Table 2; the only interatomic distance is $d(\text{B-N}) = 1.56$ Å. This distance is larger than the $d(\text{C-C})$ distance in C₈ due to the larger radius of the B atom (0.83 Å) compared to the C atom (0.77 Å); note that $r(\text{N}) = 0.75$ Å. Like C₈, the resulting 4H BN belongs to space group $P6_3mc$ and **cfc** topology.

Closer examination allowed a relationship to be established with silicon carbide. SiC is known to have 4H, 6H and 8H polytypes characterized by 4, 6 and 8 layers along the hexagonal vertical direction (cf. Figs. 2b, 2c, 2d for BN). Then, the currently calculated BN structure is a 4H polytype crystallizing in space group $P6_3mc$. In this context, hypothetical 6H and 8H BN polytypes were calculated. The second and third data columns of Table 2 give the equilibrium ground state hexagonal lattice parameters a and c , and the atomic positions of the proposed 6H and 8H polytypes. The corresponding structures are shown in Figs. 1c and 1d. The last row of Table 2 shows that all three polytypes are largely cohesive and have close $E_{\text{coh}}/\text{atom}$ values. Topology analysis led to an original **cf**d topology; 6-layered SiC polytype/chcchc (c and h indicate layer nature) for 6H BN, and "8-layered SiC polytype/chcccchc"-type for 8H BN, i.e. different from **cf**c, which defines C_8 and 4H BN. However, all BN polytypes are structurally related.

As for the ternary B-C-N compound, after the high-pressure synthesis of cubic BC_2N in 2001 [22], the orthorhombic and trigonal structures of this compound were theoretically proposed [23]. In the present work substitutions were made in the 4H BN polytype structure avoiding B-B and/or N-N bonds and favoring C-C and B-N bonds. Following these rules, the structure with these bonds shown in Fig. 1e was obtained after geometry relaxation on the ground energy, and the relevant parameters are given in the last column of Table 2. For comparison, similarities can be observed with Fig. 1f, which represents the trigonal BC_2N from previous work [23]. The interatomic distances are distributed in a range from 1.51 Å (C-N) to 1.61 Å (B-C). The structure was found to be stable with a cohesive energy between that of C_8 and BN polytypes.

Charge density

The electronic-crystal structure relationship can be further illustrated by the charge density projections with yellow volumes around atoms shown in Fig. 2. C_8 shows tetrahedral (sp^3) shape around the carbon sites, corresponding to the covalent nature of the bonds, similar to diamond. Significant changes are observed for BN: 4H, 6H and 8H polytypes (Figs. 2b-d), where charges are mainly centered on nitrogen atoms due to the higher electronegativity of N ($\chi = 3.04$) compared to B ($\chi = 2.03$), resulting in polar covalent B–N bonding. In the ternary BC_2N , the presence of carbon with intermediate electronegativity ($\chi_C = 2.55$) slightly reduces this behavior with a skewing of the charge envelopes towards C (Figs. 2e, 2f).

In the following sections, it will be shown that this charge transfer tuning has implications for the thermal properties and electronic band structures.

Mechanical properties

Elastic constants and elastic moduli

The elastic constants were calculated by performing finite distortions of the lattice around equilibrium positions. The calculated sets of elastic constants C_{ij} (i and j correspond to directions)

are given in Table 3. All C_{ij} values are positive. The elastic constants of C_8 have the largest magnitudes, close to diamond [24]. Structurally related new BN polytypes as well as wBN show the trend of decreasing C_{ij} magnitudes. Then the mechanical properties were determined from the bulk (B) and the shear (G) moduli obtained by an averaging of the elastic constants. Herein, we used Voigt's method based on a uniform strain (cf. [17] for original and modern publications). The four compounds can be differentiated from the bulk B_V and shear G_V moduli, obtained from the equations corresponding to the hexagonal system [17]:

$$B_V = 1/9 \{2(C_{11} + C_{12}) + 4C_{13} + C_{33}\}$$

$$G_V = 1/30 \{C_{11} + C_{12} + 2C_{33} - 4C_{13} + 12C_{44} + 12C_{66}\}$$

The last columns of Table 3 provides the obtained B_V and G_V . C_8 has the largest values, close to the accepted values for diamond $B_V = 445$ GPa and $G_V = 550$ GPa [24]. The three BN polytypes have close values with lower magnitudes than C_8 highlighting their similarities of structures differing by increasingly large extension. The ternaries show bulk and shear moduli closer to C_8 whence their labeling as hetero diamonds. Such trends are expected to reflect the hardness properties.

Hardness

Four modern theoretical models [25-28] have been used to predict Vickers hardness (H_V). The thermodynamic (T) model [25], which is based on thermodynamic properties and crystal structure, which generally shows good agreement with experiment, and is therefore recommended for hardness evaluation of superhard and ultrahard phases. The values of Vickers hardness and bulk moduli calculated using this model are summarized in Table 4. The Lyakhov-Oganov (LO) model [26] takes into account the topology of the crystal structure, the strength of covalent bonding, the degree of ionicity and directionality; and the empirical models, Mazhnik-Oganov (MO) [27] and Chen-Niu (CN) [28], are based on elastic properties, namely, bulk and shear moduli. As shown previously [2], in the case of superhard compounds of light elements, the Lyakhov-Oganov model gives somewhat underestimated values of hardness, while empirical models are not reliable. Fracture toughness (K_{Ic}) was evaluated using the Mazhnik-Oganov model [27]. The hardness values obtained using all four models are shown in Table 5 along with other mechanical properties.

The hardness and mechanical properties of **cf** C_8 are close to those of diamond and lonsdaleite, as expected. The corresponding values for the new BN polytypes are significantly lower and are at the level of the mechanical properties of wurtzite boron nitride, while the density, hardness and elastic moduli are practically the same for all three polytypes. As for hexagonal BC_2N , in terms of mechanical properties, it also occupies an intermediate position between C_8 and BN polytypes, with a hardness 12% lower than that of experimentally synthesized cubic BC_2N [22], and 7% lower than calculated H_V values of hypothetical orthorhombic and trigonal BC_2N [2].

Dynamic and thermal properties from the phonons

Phonon band structures

A relevant criterion of phase stability can be obtained from the dynamic properties derived from the phonon modes. The phonon energies $E = \hbar\omega$ (where \hbar is the reduced Planck constant and ω is phonon frequency) were then calculated, and the corresponding band structures were plotted along the Brillouin zone in the reciprocal space. Phonons have been calculated for C_8 , BC_2N , and 4H BN; the latter representing all three BN polytypes.

Fig. 3 shows the corresponding band structures. The bands develop along the main lines (horizontal direction) of the hexagonal Brillouin zone (reciprocal k-space;). The vertical direction shows the frequencies ω , which are given in terahertz (THz). There are $3N$ phonon total modes with 3 acoustic modes starting from zero frequency ($\omega = 0$ at the Γ point, center of the Brillouin zone), up to a few terahertz, and $3N-3$ optical modes at frequencies higher than three. The three acoustic modes correspond to the lattice rigid translation modes with two transverse modes and one longitudinal mode. In Fig 3, there are no negative frequencies, confirming that C_8 carbon allotrope (Fig. 3a), hexagonal BN polytypes (Fig. 3b) and BC_2N (Fig.3c) are dynamically stable. In C_8 (Fig. 3a), the highest band is found at $\omega \sim 40$ THz, a value observed for diamond by Raman spectroscopy [33]. For 4H BN the highest band is found at a lower frequency of ~ 38 THz. In the case of BC_2N (Fig. 3c), the introduction of C into the BN lattice results in a higher frequency band approaching 40 THz. Such observations let suggest that BC_2N should have closer behavior to C_8 , as shown above in terms of mechanical properties and thermal properties described below.

Thermodynamic properties

The thermodynamic properties of the new phases were calculated from the phonon frequencies using the statistical thermodynamic approach [34] on a high-precision sampling mesh in the Brillouin zone. The temperature dependencies of the heat capacity at constant volume (C_V) and entropy (S) of **cf** C_8 , 4H BN and hexagonal BC_2N are shown in Fig. 4 in comparison with experimental data for diamond [35,36] and wurtzite BN [37]. It is quite expected that the thermodynamic properties of **cf** C_8 and 4H BN are close to those of diamond and wurtzite BN, respectively. As for hexagonal BC_2N , its heat capacity and enthalpy, which are intermediate between C_8 and 4H BN, are in surprising agreement with the experimental data for wBN, but significantly different from the data for diamond.

Electronic band structures and density of states

Using the crystal parameters (Tables 1,2), the electronic band structures and the density of states (DOS) were obtained using the all-electrons DFT-based augmented spherical method (ASW) [19] and the GGA XC functional [11]. The left panels of Fig. 5 show the bands developing along the

main directions of the primitive hexagonal Brillouin zone. Along the vertical direction y-axis, the energy zero is taken with respect to E_V , i.e. the top of the valence band VB, which is separated from the conduction band CB by a large energy gap. As in diamond, C_8 has a band gap of $E_{\text{gap}} \sim 5$ eV. In BN, a larger band gap $E_g \approx 6$ eV is observed due to the polar covalent character, but in BC_2N the band gap $E_g \sim 5$ eV becomes closer to C_8 , indicating that the polar covalent behavior of BN (cf. Fig. 2) is less pronounced upon introduction of carbon into BN leading to the hexagonal BC_2N .

The DOS shown on the right reflect the band structures and provide further details. The x-axis corresponds to the energy with zero energy at E_V as above, and the y-axis corresponds to the DOS in $1/\text{eV}$. The two carbon sites in C_8 (Table 1) show almost identical DOS in VB and also in CB. The large charge transfer $B \rightarrow N$ is illustrated by the larger intensity N DOS versus B DOS, and their similar shapes and energy positions indicate the quantum mixing between the corresponding s- and p-valence states in the energy ranges $\{-20; -15$ eV $\}$ and $\{-10; -E_V\}$, respectively. A continuous VB characterizes BC_2N like C_8 , i.e., with enhanced covalence compared to BN due to the presence of C. The DOS are characterized by high intensity N(2s) at ~ -20 eV and N(2p) ~ -7 eV. Quantum mixing is now observed for all three atomic constituents, marking the chemical bonding between them.

Conclusions

Based on **cfc** carbon allotrope C_8 , novel dense hexagonal sp^3 -bonded BN polytypes (4H, 6H, 8H) and BC_2N have been proposed from crystal chemistry and first principles. All new phases were found to be superhard, mechanically and dynamically stable, with band structures characterized by large gaps, similar to diamond.

Author Contributions: Conceptualization, S.F.M.; methodology, S.F.M. and V.L.S.; validation, S.F.M. and V.L.S.; formal analysis, S.F.M. and V.L.S.; investigation, S.F.M. and V.L.S.; resources, S.F.M.; data curation, S.F.M. and V.L.S.; writing—original draft preparation, S.F.M.; writing—review and editing, V.L.S.; visualization, S.F.M. and V.L.S. All authors have read and agreed to the published version of the manuscript.

Funding: This research received no external funding.

Data Availability Statement: The data presented in this study are available on request.

Conflicts of Interest: The authors declare no conflict of interest.

References

- [1] Solozhenko, V.L. High-pressure synthesis of novel superhard phases. in: *Comprehensive Hard Materials* (eds. V.K. Sarin and C.E. Nebel), Elsevier, 2014, pp. 641-652.
- [2] Solozhenko, V.L.; Matar, S.F. Prediction of novel ultrahard phases in the B–C–N system from first principles: Progress and problems. *Materials* **2023**, *16*, 886.
- [3] Shevchenko, A.P.; Shabalin, A.A.; Karpukhin, I.Y.; Blatov, V.A. Topological representations of crystal structures: generation, analysis and implementation in the TopCryst system. *STAM: Methods* **2022**, *2*, 250-265.
- [4] Öhrström, L.; O'Keeffe, M. Network topology approach to new allotropes of the group 14 elements. *Z. Kristallogr.* **2013**, *228*, 343-346.
- [5] Gil, B.; Desrat, W.; Rousseau, A.; Elias, C.; Valvin, P.; Moret, M.; Li, J.; Janzen, E.; Edgar, J.H.; Cassabois, G. Polytypes of sp²-bonded boron nitride. *Crystals* **2022**, *12*, 782.
- [6] Hohenberg, P.; Kohn, W. Inhomogeneous electron gas. *Phys. Rev. B* **1964**, *136*, 864-871.
- [7] Kohn, W.; Sham, L.J. Self-consistent equations including exchange and correlation effects. *Phys. Rev. A* **1965**, *140*, 1133-1138.
- [8] Kresse, G.; Furthmüller, J. Efficient iterative schemes for ab initio total-energy calculations using a plane-wave basis set. *Phys. Rev. B* **1996**, *54*, 11169.
- [9] Kresse, G.; Joubert J. From ultrasoft pseudopotentials to the projector augmented wave. *Phys. Rev. B* **1994**, *59*, 1758-1775.
- [10] Blöchl, P.E. Projector augmented wave method. *Phys. Rev. B* **1996**, *50*, 17953-17979.
- [11] Perdew, J.; Burke, K.; Ernzerhof, M. The Generalized Gradient Approximation made simple. *Phys. Rev. Lett.* **1996**, *77*, 3865-3868.
- [12] Heyd, J.; Scuseria, G.E.; Ernzerhof, M. Hybrid functionals based on a screened Coulomb potential. *J. Chem. Phys.* **2006**, *124*, 219906.
- [13] Press, W.H.; Flannery, B.P.; Teukolsky, S.A.; Vetterling, W.T. *Numerical Recipes*. Cambridge University Press: New York, 1986.
- [14] Blöchl, P.E.; Jepsen, O.; Anderson, O.K. Improved tetrahedron method for Brillouin-zone integrations. *Phys. Rev. B* **1994**, *49*, 16223-16233.
- [15] Methfessel, M.; Paxton, A.T. High-precision sampling for Brillouin-zone integration in metals. *Phys. Rev. B* **1989**, *40*, 3616-3621.
- [16] Monkhorst, H.J.; Pack, J.D. Special k-points for Brillouin Zone integration. *Phys. Rev. B* **1976**, *13*, 5188-5192.

- [17] Voigt, W. Über die Beziehung zwischen den beiden Elasticitätsconstanten isotroper Körper. *Ann. Phys.* **1889**, 274, 573-587; Blaschke, D.N. Averaging of elastic constants for polycrystals. *J. Appl. Phys.* **2017**, 122, 145110.
- [18] Togo, A.; Tanaka, I. First principles phonon calculations in materials science, *Scr. Mater.* **2015**, 108, 1-5.
- [19] Momma, K.; Izumi, F. VESTA3 for three-dimensional visualization of crystal, volumetric and morphology data. *J. Appl. Crystallogr.* **2011**, 44, 1272-1276.
- [20] Eyert, V. Basic notions and applications of the augmented spherical wave method. *Int. J. Quantum Chem.* **2000**, 77, 1007-1031.
- [21] Bundy, F.P.; Kasper, J.S. Hexagonal diamond – A new form of carbon. *J. Chem. Phys.* **1967**, 46, 3437-3446.
- [22] Solozhenko, V.L.; Andrault, D.; Fiquet, G.; Mezouar, M.; Rubie D.C. Synthesis of superhard cubic BC₂N. *Appl. Phys. Lett.* **2001**, 78, 1385-1387.
- [23] Mattesini, M.; Matar, S.F. First-principles characterisation of new ternary heterodiamond BC₂N phases. *Comput. Mater. Sci.* **2001**, 20, 107-119.
- [24] Brazhkin, V.V.; Solozhenko, V.L. Myths about new ultrahard phases: Why materials that are significantly superior to diamond in elastic moduli and hardness are impossible. *J. Appl. Phys.* **2019**, 125, 130901.
- [25] Mukhanov, V.A.; Kurakevych, O.O.; Solozhenko, V.L. The interrelation between hardness and compressibility of substances and their structure and thermodynamic properties. *J. Superhard Mater.* **2008**, 30, 368-378.
- [26] Lyakhov, A.O.; Oganov, A.R. Evolutionary search for superhard materials: Methodology and applications to forms of carbon and TiO₂. *Phys. Rev. B* **2011**, 84, 092103.
- [27] Mazhnik, E.; Oganov, A.R. A model of hardness and fracture toughness of solids. *J. Appl. Phys.* **2019**, 126, 125109.
- [28] Chen, X-Q.; Niu, H.; Li, D.; Li, Y. Modeling hardness of polycrystalline materials and bulk metallic glasses. *Intermetallics*, **2011**, 19, 1275-1281.
- [29] Bindzus, N.; Straasø, T.; Wahlberg, N.; Becker, J.; Bjerg, L.; Lock, N.; Dippel, A.-C.; Iversen, B.B. Experimental determination of core electron deformation in diamond. *Acta Cryst. A* **2014**, 70, 39-48.
- [30] Ownby, P.D.; Yang, X.; Liu, J. Calculated X-ray diffraction data for diamond polytypes. *J. Am. Ceram. Soc.* **1992**, 75, 1876-1883.
- [31] Kurdyumov, A.V.; Solozhenko, V.L.; Zelyavski, W.B. Lattice parameters of boron nitride polymorphous modifications as a function of their crystal-structure perfection. *J. Appl. Crystallogr.* **1995**, 28, 540-545.

- [32] Solozhenko, V.L.; Häusermann, D.; Mezouar, M.; Kunz, M. Equation of state of wurtzitic boron nitride to 66 GPa. *Appl. Phys. Lett.* **1998**, *72*, 1691-1693.
- [33] Krishnan, R.S. Raman spectrum of diamond. *Nature* **1945**, *155*, 171.
- [34] Dove, M.T. *Introduction to lattice dynamics*. Cambridge University Press, 1993.
- [35] DeSorbo, W. Specific heat of diamond at low temperatures. *J. Chem. Phys.* **1953**, *21*, 876-880.
- [36] Victor, A.C. Heat capacity of diamond at high temperatures. *J. Chem. Phys.* **1962**, *36*, 1903-1911.
- [37] Solozhenko, V.L.; Gavrichev, K.S. Thermodynamic properties of boron nitride. in: "*Wide Band Gap Electronic Materials*". (eds. M.A. Prelas et al.), Kluwer Academic Publishers: Dordrecht, Netherlands, 1995, pp. 377-392.

Table 1. Crystal structure parameters of template hexagonal C₈ (**cfc** topology) in two space groups.

	<i>P6₃/mmc</i> (No. 194)*	<i>P6₃mc</i> (No. 186)
<i>a</i> , Å	2.512 (2.512)	2.505
<i>c</i> , Å	8.295 (8.266)	8.338
<i>V_{cell}</i> , Å ³	45.24 (45.21)	45.31
$\langle V_{atom} \rangle$, Å ³	5.66 (5.66)	5.66
Shortest <i>d-d</i> , Å	1.54 (1.54)	1.54
Atomic positions	C1 (4e) 0, 0, 0.093 (<i>z</i> = 0.093) C2 (4f) 2/3, 1/3, 0.156 (<i>z</i> = 0.155)	C1 (2a) 0, 0, 0.0934 C2 (2a) 0, 0, 0.9070 C3 (2b) 2/3, 1/3, 0.156 C4 (2b) 1/3, 2/3, 0.6558
<i>E_{total}</i> , eV	-72.68	-72.68
<i>E_{coh}/atom</i> , eV	-2.49	-2.49

* The values in brackets are literature data [4].

Table 2. Crystal structure parameters of hexagonal (*P6₃mc*, No. 186) BN polytypes and BC₂N

	4H BN (<i>Z</i> = 4)	6H BN (<i>Z</i> = 6)	8H BN (<i>Z</i> = 8)	BC ₂ N (<i>Z</i> = 2)
<i>a</i> , Å	2.545	2.547	2.548	2.525
<i>c</i> , Å	8.363	12.529	16.693	8.413
<i>V_{cell}</i> , Å ³	46.94	70.39	93.84	46.47
Shortest <i>d-d</i> , Å	1.56 (B-N)	1.56 (B-N)	1.56 (B-N)	1.51 (C-N) 1.54 (C-C) 1.56 (B-N) 1.62 (B-C)
Atomic position	B1 (2a) 0, 0, 0.0934 B2 (2b) 2/3, 1/3, 0.3440 N1 (2a) 0, 0, 0.9068 N2 (2b) 1/3, 2/3, 0.6558	B1 (2a) 0, 0, 0.4999 B2 (2b) 1/3, 2/3, 0.1666 B3 (2b) 1/3, 2/3, 0.8326 N1 (2a) 0, 0, 0.3743 N2 (2b) 1/3, 2/3, 0.0419 N3 (2b) 1/3, 2/3, 0.7080	B1 (2a) 0, 0, 0.00021 B2 (2b) 1/3, 2/3, 0.2499 B3 (2b) 1/3, 2/3, 0.6249 B4 (2b) 1/3, 2/3, 0.8755 N1 (2a) 0, 0, 0.0938 N2 (2b) 1/3, 2/3, 0.3442 N3 (2b) 1/3, 2/3, 0.7185 N4 (2b) 1/3, 2/3, 0.9690	B (2b) 2/3, 1/3, 0.3461 N (2a) 0, 0, 0.9113 C1 (2a) 0, 0, 0.0915 C2 (2b) 1/3, 2/3, 0.6512
<i>E_{total}</i> , eV	-69.62	-104.46	-139.29	-69.75
<i>E_{coh}/atom</i> , eV	-2.65	-2.66	-2.65	-2.39

Table 3. Elastic constants, bulk B_V and shear G_V moduli of new phases (all values are in GPa).

	C_{11}	C_{12}	C_{13}	C_{33}	C_{44}	C_{66}	B_V	G_V
cfc C_8 ^{#194}	1167	127	39	1269	520	471	446	518
wBN ^{#186}	963	144	61	1064	406	337	397	390
4H BN ^{#186}	939	154	71	1032	393	347	389	392
6H BN ^{#186}	945	143	73	1022	401	349	388	395
8H BN ^{#186}	933	166	77	1008	383	339	390	382
<i>h</i> -BC ₂ N ^{#186}	1048	128	46	1110	460	397	405	450

Table 4. Vickers hardness (H_V) and bulk moduli (B_0) calculated within the thermodynamic model of hardness [25].

	Space group	$a = b$ (Å)	c (Å)	ρ (g/cm ³)	H_V (GPa)	B_0 (GPa)
Diamond	<i>Fd-3m</i>	3.56661 ^a		3.517	98	445 ^b
Lonsdaleite	<i>P6₃/mmc</i>	2.5221 ^c	4.1186 ^c	3.516	97	443
cfc C_8 ^{#194}	<i>P6₃/mmc</i>	2.5115	8.2824	3.527	98	446
wBN ^{#186}	<i>P6₃/mc</i>	2.5505 ^d	4.2100 ^d	3.475	54	373 ^e
4H-BN ^{#186}	<i>P6₃/mc</i>	2.5454	8.3653	3.512	56	380
6H-BN ^{#186}	<i>P6₃/mc</i>	2.5470	12.529	3.513	56	380
8H-BN ^{#186}	<i>P6₃/mc</i>	2.5477	16.693	3.513	56	380
<i>h</i> -BC ₂ N ^{#186}	<i>P6₃/mc</i>	2.5254	8.4133	3.491	67	402

^a Ref. 29.

^b Ref. 24.

^c Ref. 30.

^d Ref. 31.

^e Ref. 32.

Table 5. Mechanical properties: Vickers hardness (H_V), bulk modulus (B), shear modulus (G), Young's modulus (E) (all values are in GPa), Poisson's ratio (ν) and fracture toughness (K_{Ic}) (in $\text{MPa}\cdot\text{m}^{1/2}$)

	H_V				B		G_V	E^e	ν^e	K_{Ic}^c
	T^a	LO^b	MO^c	CN^d	B_0^a	B_V				
	GPa									
Diamond	98	90	100	93	445 ^f		530 ^f	1138	0.074	6.4
Lonsdaleite	97	90	99	94	443	432	521	1115	0.070	6.2
cf C_8 ^{#194}	98	90	97	96	446	446	518	1122	0.081	6.4
wBN ^{#186}	54	50	72	65	373 ^g	390	397	889	0.120	5.1
4H-BN ^{#186}	56	51	70	69	380	389	392	880	0.123	5.1
6H-BN ^{#186}	56	51	71	71	380	388	395	884	0.120	5.0
8H-BN ^{#186}	56	51	67	69	380	390	382	865	0.131	5.5
<i>h</i> - BC_2N ^{#186}	67	56	83	78	402	405	450	985	0.095	5.4

^a Thermodynamic model [25]

^b Lyakhov-Oganov model [26]

^c Mazhnik-Oganov model [27]

^d Chen-Niu model [28]

^e E and ν values calculated using isotropic approximation

^f Ref. 24.

^g Experimental value $B_0 = 375(9)$ GPa [32]

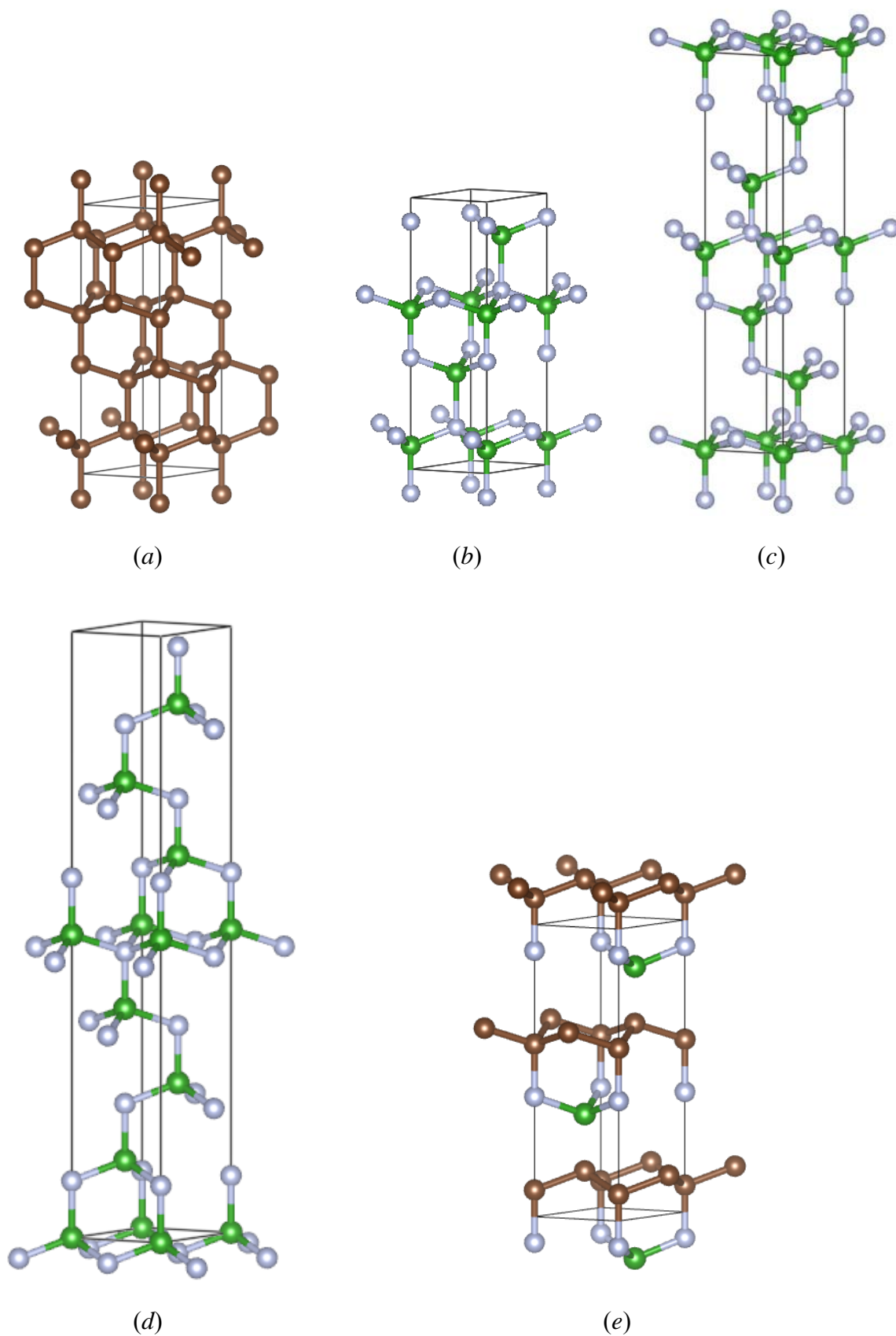


Fig. 1. Sketches of the crystal structures of **cfc** C₈ (a), 4H (b), 6H (c) and 8H (d) BN polytypes, and hexagonal BC₂N (e). Green, brown and grey spheres correspond to B, C and N atoms, respectively.

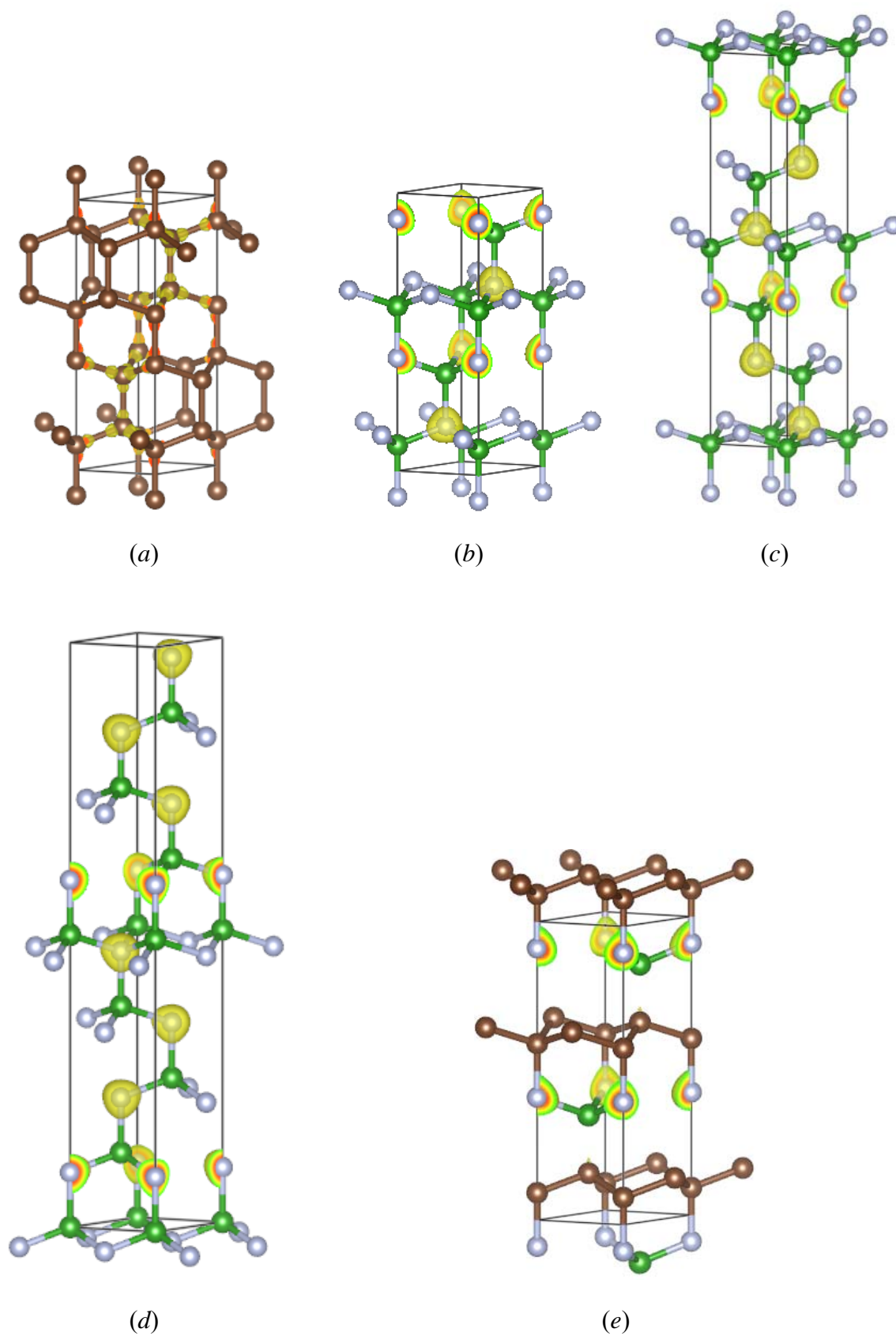


Fig. 2. Charge density projections (yellow volumes) of **cfc** C₈ (a), 4H (b) and 6H (c), 8H (d) BN polytypes, and hexagonal BC₂N (e). Green, brown and grey spheres correspond to B, C and N atoms, respectively.

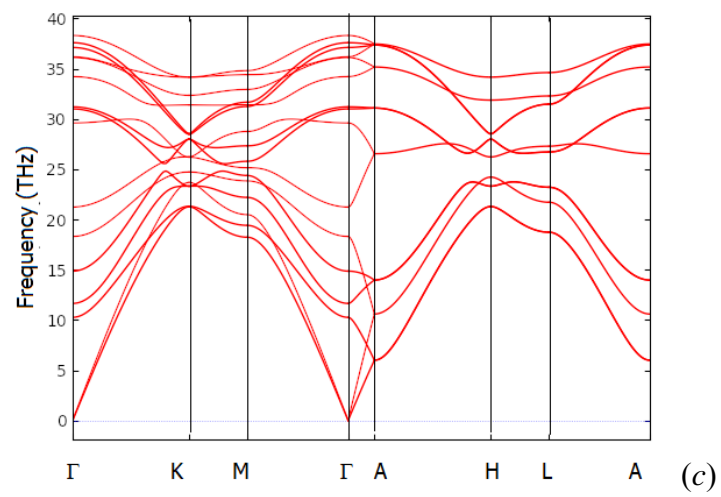
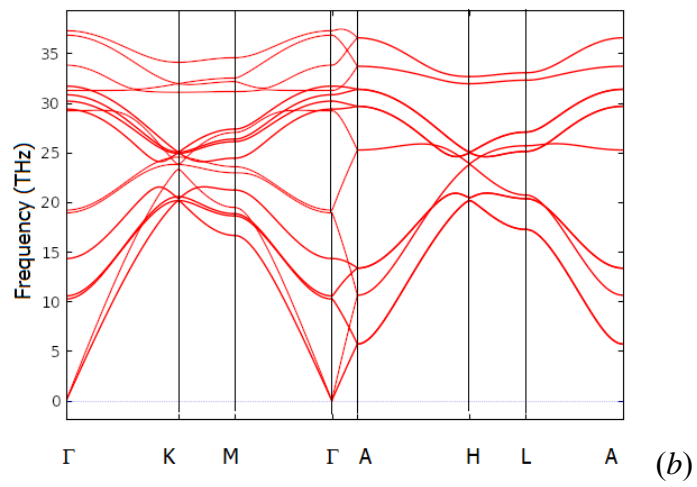
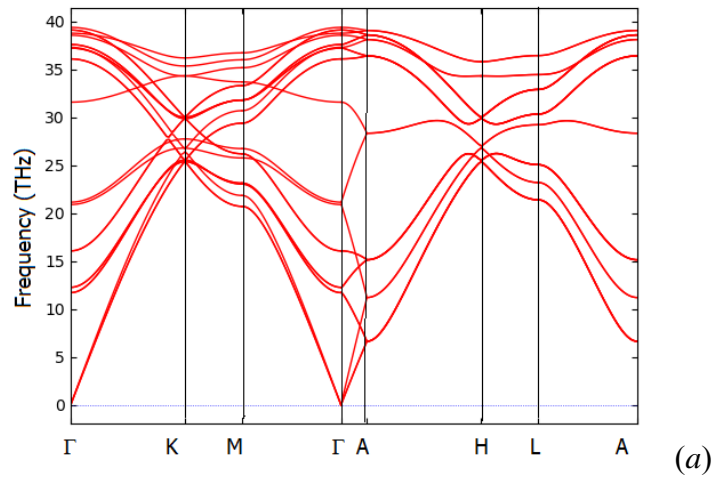
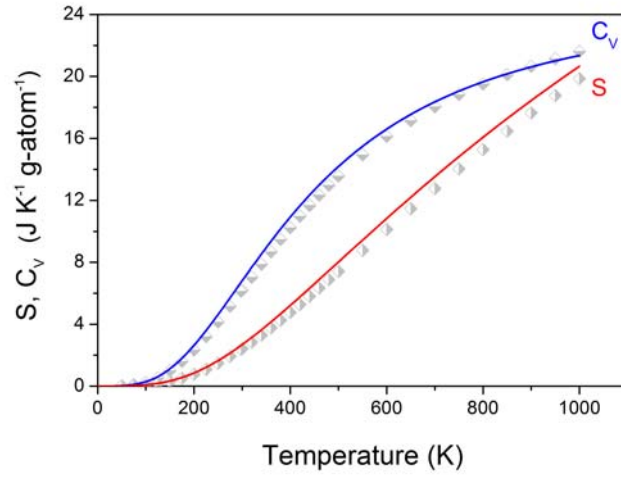
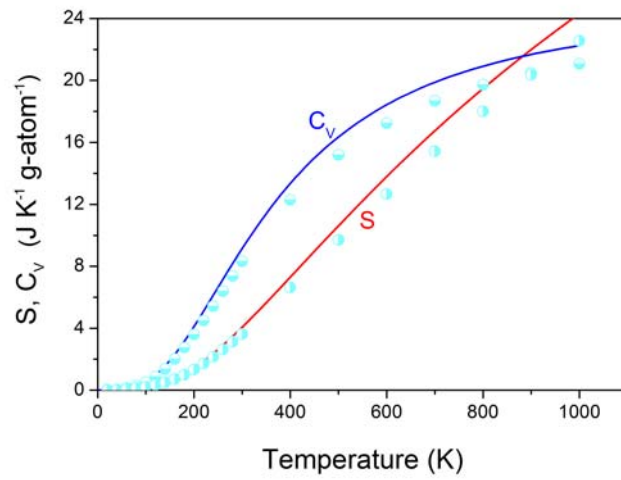


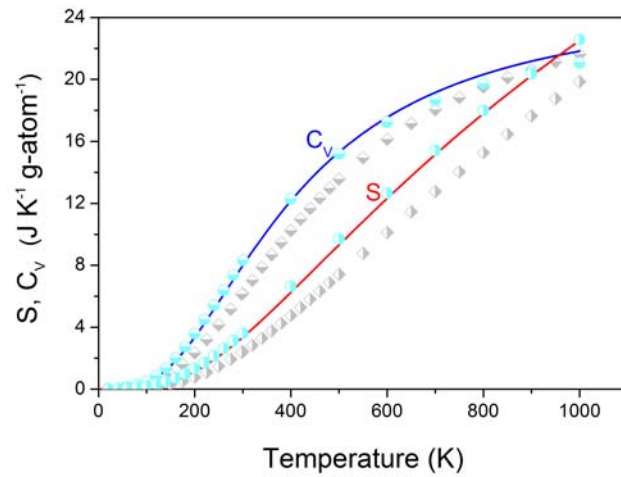
Fig. 3. Phonon band structures of **cfc** C_8 (a), 4H BN polytype (b) and hexagonal BC_2N (c)



(a)



(b)



(c)

Fig. 4. Heat capacity at constant volume and entropy of **cfc** C_8 (a), 4H BN polytype (b) and hexagonal BC_2N (c) as functions of temperature. Experimental data for diamond [35,36] and wurtzite BN [37] are shown as gray and cyan symbols, respectively.

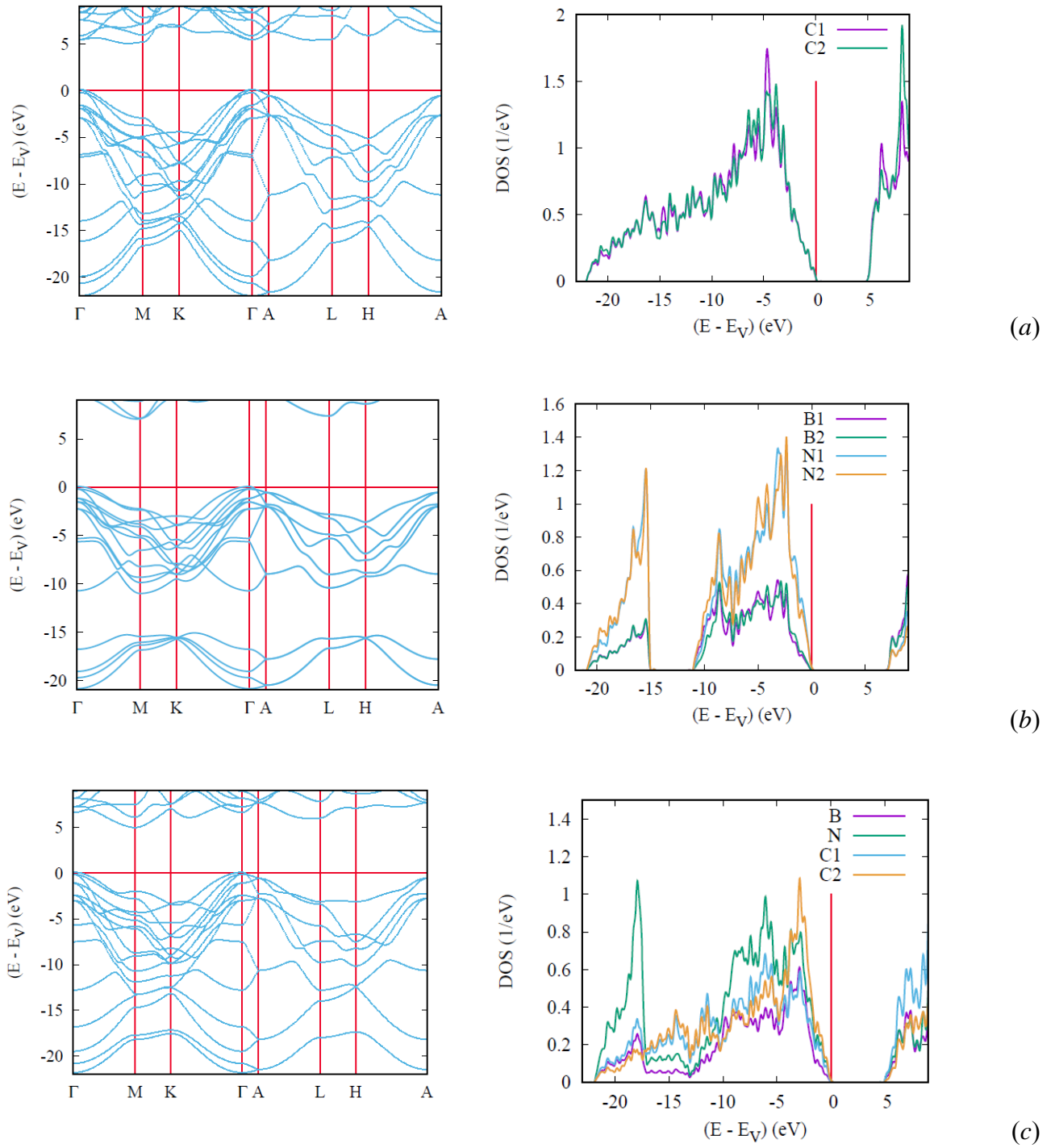


Fig. 5. Electronic band structures (left) and site projected density of states (right) of **cfc C₈** (a), 4H BN polytype (b) and hexagonal BC₂N (c).